Chemical Engineering Journal 159 (2010) 159–169

Contents lists available at ScienceDirect

Chemical Engineering Journal

journal homepage: www.elsevier.com/locate/cej

Experimental demonstration of rotating spiral microchannel distillation

J.M. MacInnes*, J. Ortiz-Osorio[1], P.J. Jordan[2], G.H. Priestman, R.W.K. Allen

Department of Chemical and Process Engineering, University of Sheffield, Newcastle Street, Sheffield S1 3JD, UK

ARTICLE INFO

Article history:
Received 28 September 2009
Received in revised form 21 January 2010
Accepted 15 February 2010

Keywords:
Distillation
Phase contacting
Microchannel
Mass transfer
Centrifugal
Coriolis
Intensification

ABSTRACT

A prototype device using a rotating spiral microchannel to produce multistage distillation has been designed and used to separate 2,2-dimethylbutane from an initial 50:50 mixture with 2-methyl-2-butene. Distillation or other phase-contacting processes in microchannels requires a strategy for handling surface forces so that the phases can interact in a controlled manner and efficient mass transfer can take place. The rotating spiral approach uses centrifugal force to maintain segregation of the phases into parallel-flowing liquid and vapour layers. When centrifugal force is opposed by pressure gradient along the channel, these layers can flow counter currently. Changing rotation rate and pressure allows adjustment of the phase flow rates and the contacting layer thicknesses. Thus, it is possible to control the phase contacting and take full advantage of the rapid mass transfer that is potentially available for small microchannel dimensions. This efficient contact can be maintained over long channel distances, allowing a large number of separation stages to be reached. A further advantage of the rotating spiral approach is that the mass transfer is augmented by secondary motions produced by Coriolis force. The paper describes the design of the prototype device, including flow and thermal aspects, and presents results for a simple binary distillation. The results obtained demonstrate the practical feasibility of rotating spiral contacting and provide initial quantitative data that are used to evaluate the performance achieved by the prototype device.

1. Introduction

Fluid phase contacting is a central problem in the area of separation of molecular species from a mixture of multiple species and forms the basis for such processing operations as absorption, extraction and distillation. Recently, interest has been directed at implementing such operations in microscale analytical and processing devices [1–4]. The phases may be immiscible liquids, a gas and a liquid or combinations of these. It is well known that precise separation depends on counter-current flow of the phases as they contact one another [5,6], otherwise the enrichment produced is limited by the equilibrium concentrations in the two phases. Conventionally, gravity is used to drive the liquid phase downward and the vapour phase is driven upward by imposed pressure difference to produce the required counter flow. However, at the small scales of a microchannel, gravity is weak both in terms of driving the flow against friction and in terms of countering surface forces that tend to collect the vapour into pockets and the liquid into slugs that span the entire channel section, preventing effective counter-current flow.

The objective of the present work is to introduce and demonstrate a novel method of contacting fluid phases in which the phases are made to flow counter currently along a microchannel in parallel layers controlled by centrifugal force and pressure gradient. The method can in principle be applied to the entire range of phase-contacting types, but here it is applied to distillation, arguably the most difficult to implement due to the additional complexities associated with the requirements of thermal control. Equally, there is no reason that the approach cannot be scaled up to the point beyond which the phase layers are no longer stable. By forming the contacting microchannel into a spiral and rotating this spiral about its axis (Fig. 1) centrifugal acceleration occurs having components both along the channel and perpendicular to the channel. The division between the two components depends on the spiral angle, i.e. the angle between the channel direction and the tangential direction. The perpendicular component is used to counter surface force and organise the phases into the parallel layers and therefore relying on a difference in density between the phases. In place of gravity, the component of centrifugal acceleration along the channel drives the liquid outward along the spiral and the vapour can flow inward, with appropriate adjustment of the pressure gradient.

Coriolis force also plays a role in the phase contacting, acting on the fluids in the direction approximately perpendicular both to the

* Corresponding author. Tel.: +44 114 222 7511; fax: +44 114 222 7501.
E-mail address: j.m.macinnes@sheffield.ac.uk (J.M. MacInnes).
[1] Permanent address: Chrysler Corporate Headquarters at Mexico City, Prolongación Paseo de la Reforma 1240, Santa Fe, Mexico City 05109, Mexico.
[2] Permanent address: Department of Chemical and Process Engineering, University of Canterbury, New Zealand.

1385-8947/$ – see front matter © 2010 Elsevier B.V. All rights reserved.
doi:10.1016/j.cej.2010.02.030

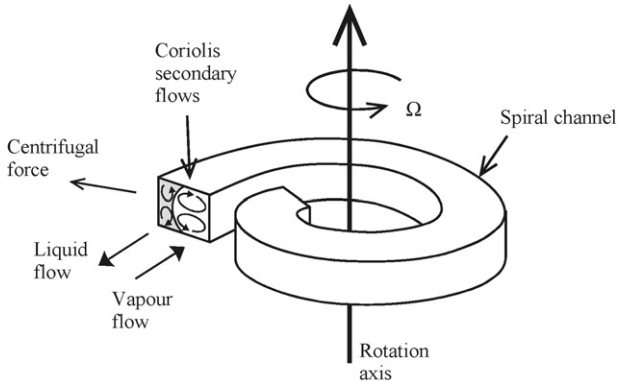

Fig. 1. Phase contacting in a rotating spiral microchannel.

channel direction and the axis of rotation. This is because the Coriolis force per unit volume of fluid is $-2\rho\bar{\Omega} \times \bar{V}$ where ρ is local fluid density, $\bar{\Omega}$ is the angular velocity vector and $\bar{V}$ the fluid velocity vector in the rotating frame [7]. This force is proportional to both the rotation rate and fluid velocity. Because the velocity is not uniform over a cross-section of the channel, high in the core regions of each phase and low near the walls, the Coriolis force induces 'secondary' convective motions such as those illustrated in Fig. 1. The nature of these motions has been extensively investigated because of their importance for gas turbines, where coolant channels run through the rotating turbine blades. Laminar flow and heat transport in rotating channels has been studied [8–10] and the magnitude of the Coriolis secondary velocity relative to the streamwise velocity has been shown to increase with Reynolds number [11]. Most investigations of the Coriolis secondary motions to date have looked at flow stability [12–14] and the fully turbulent flow regime [15,16], neither of which is directly relevant to the usual flow conditions in small-scale channels. Computations by the authors for the liquid phase indicate that the Coriolis motions produce a significant improvement in mass transfer even at the low Reynolds number conditions of the present experiments [17].

Other approaches to phase contacting have also used centrifugal force to replace gravity but have employed the conventional approach of driving bubbles or droplets of one phase through the other. In the HIGEE approach, a rotating packed bed is employed to increase the phase flow rates per bed area [18–20]. Counter-current chromatography has been taken to high precision using planetary gearing to rotate a coil of tubing (helical channel) to produce contacting between two immiscible liquids characterised by alternating layered flow and flow in which the phases are mixed [21,22]. While a high number of separation stages is achieved, the device complexity may be of some concern. In both these approaches the phases are driven through one another, requiring first generation of either bubbles or droplets of one phase, then forcing these through the other phase and finally separating the phases to allow the product flows to be formed. The dynamics of bubble and droplet formation depend strongly on fluid and interface properties as well as phase flow conditions, so successful operation can be highly constrained in these approaches.

A related technology to that addressed here is compact disk (CD)-based microfluidics which has been under development in recent years [23–27]. Essentially, for disposable 'point of use' analyses the usual pumping methods are viewed as expensive and inconvenient and are replaced by centrifugal pumping. The required solutions for the analysis (e.g. sample, wash, calibration) are introduced into inlets of a suitable microchannel network on a CD, the CD is inserted into a disk drive and the required flow sequence for sample analysis is produced by control of rotation rate with time. Coriolis acceleration has been used to assist the mixing of the liquids and to switch the liquid flow at a branch junction [25]. In this method, separating particles from a liquid stream is easily achieved by the centrifugal force [26,27]. Otherwise, functioning is as for a stationary device but with pumping produced by centrifugal force in place of, for example, syringes or application of pneumatic pressure.

Relatively little work on distillation in microchannel devices has yet been reported. In some work, co-flow of the phases is accepted [1,3], thus limiting separation to just one equilibrium stage. It is argued that more precise separation can be achieved by linking together multiple units, with associated pumps to produce the necessary counter-current flows between the individual units. Wootton et al. [1] use a complex network and helium carrier gas to produce one stage of distillation, first by evaporating an acetonitrile–dimethylformamide mixture into the carrier gas and then condensing and separating the liquid phase from the vapour and carrier gas mixture. Hartman et al. [3] use nitrogen carrier gas and segmented flow in a long heated channel to produce equilibrium between the liquid and vapour at a prescribed temperature. The liquid is separated from the vapour and carrier gas using a PTFE membrane, which allows the liquid to pass through but not the gases when the pressures on either side of the membrane are suitably adjusted.

Multiple stages of separation in a single device, as mentioned, requires counter flow and one method of achieving this is to use a film of liquid falling under gravity. The vapour flow can then be forced by pressure gradient to flow vertically as it contacts the falling film. Tonkovich et al. [2] describe the 15 stage separation of cyclohexane–hexane using a falling film arrangement in which a 178 μm liquid layer is stabilised using a woven wire mesh adjacent to a 1.35 mm gas layer flowing counter currently. Each stage requires 8.3 mm of channel length. Stabilisation of the liquid layer using a vertical grooved plate has also been employed [28–30]. Surface forces and the sharp edges of the grooves compel the liquid to remain within the grooves and gravity again drives the liquid downward. This approach has been developed in relation to gas/liquid microreactors and only the case of a co-flowing gas has been investigated, although it would clearly be possible to drive the gas in counter-current flow simply by changing the direction of the pressure gradient. The use of gravity to drive flow at small scales necessarily limits the achievable flow rates to modest levels.

Alternatively, multiple stages can be achieved using a membrane barrier to maintain segregation of the liquid and vapour phases in counter-current flow. A membrane with suitable pore size and shape and of appropriate material prevents the liquid from crossing. Pressure gradient is required to drive the flow along the channels on both sides of the membrane, leading to a rising pressure along the channel in one phase but a falling pressure along the channel in the other phase and consequently a varying pressure difference across the membrane. The presence of the membrane introduces additional resistance to both heat and mass transfer and fouling can be an issue [31]. Cypes and Engstrom [32] report stripping of toluene from a water–toluene mixture into a nitrogen stream employing a microfabricated membrane device. The membrane comprises a regular array of 50 μm connecting holes etched through the silicon layer separating the liquid and gas channels. Zhang et al. [4] produce vacuum membrane distillation of a water-methanol mixture using a microchannel device incorporating a PTFE membrane. A cooling channel is used to regulate temperature along the contacting channels. The device produces just 1.7 stages of distillation for the 260 mm long contacting channel. This performance is far lower than for the falling film distillation mentioned above [4], which would give about 30 stages for the same channel length.

Rotating spiral contacting overcomes the limitations of gravity flow and simplifies phase interaction to that between two parallel-

flowing layers. Mass transfer between the phases is determined by the layer thicknesses, the velocity field and the diffusivity in each phase, along with the liquid–vapour equilibrium characteristics of the mixture. The velocity and layer thicknesses are controlled by spiral angle, rotation rate and pressure gradient. This means that adjustment of rotation rate and pressure gradient can be used to change the velocities and thicknesses of the phases and hence to control the mass transfer during processing to accommodate the requirements of each particular fluid system. Also, the layer thicknesses and velocities can remain constant over the entire length of the spiral so that the mass transfer is controlled with each element of liquid or vapour being an active participant at all times during passage through the contacting channel.

Efficient distillation at microchannel scale opens the way for improved analytical and small-scale production devices. High heat and mass transfer rates and small timescales allow high precision separation in a short time: minutes where a conventional separation requires hours. The high transfer rates can allow many separation stages with results obtained rapidly. The small time scale further means that changes in the operating conditions, e.g. start-up or switching from one operating state to another, are rapid. The time taken for species to transfer between the phase interface and the adjacent regions of liquid and vapour determines how rapidly separation can take place. Assuming that the transfer of species is by diffusion alone, the characteristic time taken for species to become uniform over the distance of the channel width, W, is $\tau = W^2/D$ where D is the relevant diffusion coefficient. For a 10 μm channel for example, $\tau = 0.1$ s for a diffusivity in the liquid phase of $D = 10^{-9}$ m^2/s (a usual level for small molecules in 'thin' liquids). Thus, 100 stages of distillation would take 10 s. Increasing channel size to 100 μm would require 15 min for the same distillation. The diffusion time scale used for these estimates is conservative and the actual diffusion times will be even shorter. Also, no account has been taken of the effect of Coriolis convection, which will reduce the mass transfer time scale further, the effect increasing with channel size. In practical devices, the limiting process is likely to be not the mass transfer occurring within the small channel but rather the heat transfer throughout the device, which is important for many contacting operations. Careful design of the overall device will be important if the potential of rapid adjustment is to be fully achieved.

The paper describes the first successful distillation of a binary mixture (2-methyl-2-butene and 2,2-dimethylbutane) using a rotating spiral microchannel to contact the phases. The design of the experimental device is described along with some key theoretical results and details of the concept used that are judged necessary to understanding the results presented. This includes a description of how the flow circuit was designed and an account of how the heating and cooling rates to produce a satisfactory temperature field were determined.

2. Experimental

2.1. Apparatus

The demonstration device uses a largely self-contained rotating unit to produce stripping distillation. The rotating unit incorporates a central feed reservoir, two outer collection reservoirs, a glass chip incorporating the spiral microchannels and heating and cooling elements. Liquid feed mixture is pumped by centrifugal force when rotation is introduced. The device is constructed with appropriate geometric symmetry so that it is well balanced dynamically under rotation. The assembly is rotated by direct drive with a 24 V DC motor (Maxon EC45) capable of 10,000 rpm, although the experiments considered here are all at 5000 rpm. The motor is mounted on an overhanging bracket such that the rotating experiment is suspended above an inverted microscope (Zeiss Axiovert 100 with Epiplan 5×/0.13 objective lens), allowing visual observation of the flow during rotation. The rotating unit is self-contained except that the electrical power required for heating is transferred from an external DC supply (TTi EX354D) using commercial slip rings (Fabricast Type 1926). The overall apparatus is shown in Fig. 2.

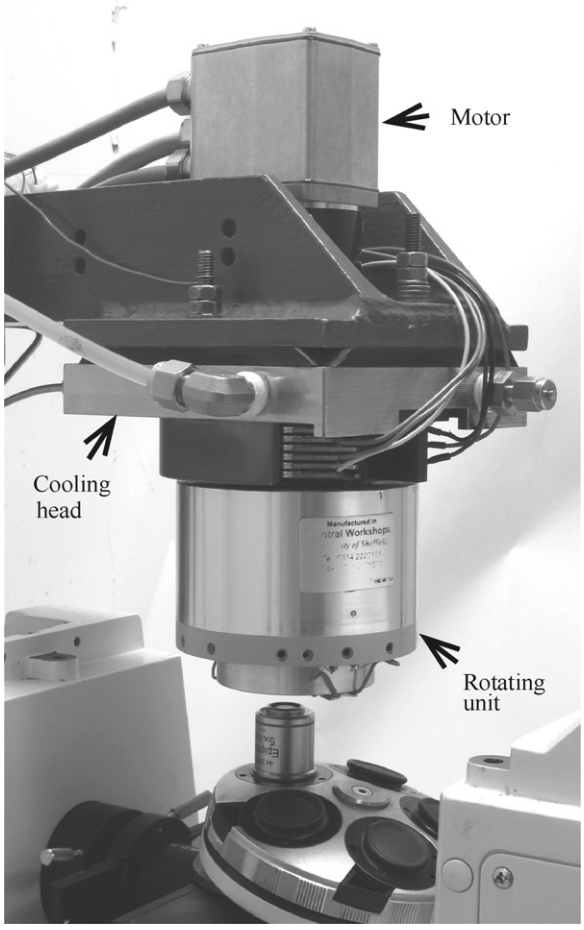

Fig. 2. General view of the apparatus.

The spiral channel network is formed by isotropic wet etching through a mask pattern into 2.3 mm thick optical glass. Access holes are drilled and the channels are enclosed by thermal bonding of a second 1 mm thick optical glass layer. The completed chip is shown in Fig. 3. A binary liquid mixture enters at the feed inlet, increases in temperature as it travels along the inlet channel, reaching its bubble point temperature at the junction and then flowing along the outer side of the spiral contacting channel. A radially increasing temperature is imposed on the glass chip so that as the liquid flows out along the contacting channel its temperature rises and eventually becomes high enough to boil the liquid (i.e. the local temperature of the chip exceeds the local bubble point sufficiently to produce strong evaporation). This evaporation tends to increase the pressure which drives vapour back up the spiral alongside and counter currently to the liquid and out through the junction to the inner, vapour channel. The contacting spiral and the vapour spiral lead to the bottom and top outlet holes respectively via wide channels to assist condensation, which produces liquid product flows. Temperature decreases in the radial direction in the outer part of the chip beginning at a radial location that is about where the spirals join the wide condensing channels. All channels are etched to a depth of 95 μm and the spiral channels are 250 μm wide (the

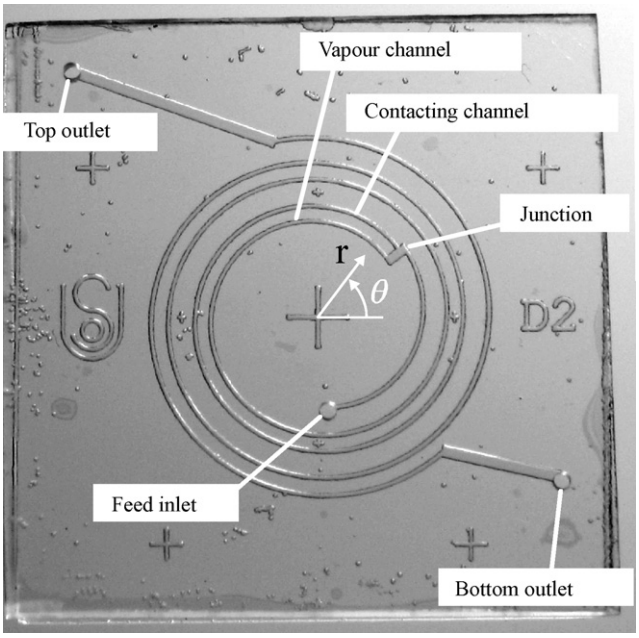

Fig. 3. Glass chip fabricated from two glass layers. The 2.3 mm top layer is isotropically etched to form the channels, holes are drilled for flow access and it is thermally bonded to a 1 mm bottom layer to complete the chip. The overall size is 40 mm × 40 mm; the spiral channels are 255 μm wide and 95 μm deep and the inlet and outlet holes are 1 mm diameter.

condenser channels are 800 μm wide and the junction channel is 500 μm wide). The spirals used are such that $r \sin\alpha = 0.00539$ m, which as will be indicated ensures a constant body force and hence constant liquid layer thickness along the contacting spiral.

The chip is held in a base unit containing the flow and heating apparatus (Fig. 4) and this screws into a rotating top unit (Fig. 2) which in turn is directly fixed to the motor using a locking bush (Tollok TLK110 8 mm). Fig. 4 shows two views of the assembled base unit. On top are collection vials for the top and bottom outlet flows and a central feed reservoir. The feed reservoir has a cylindrical internal shape (not shown) and an atmospheric vent concentric with the rotation axis. Under rotation a cylindrical atmospheric free surface forms in the reservoir. Liquid flows between the feed reservoir and the chip and between the chip and the vials through PEEK capillary tubing with connections made using NanoPort fittings (Upchurch). The feed tubing has a 150 μm internal diameter and the top and bottom connecting tubing has 50 μm internal diameter. The vials each have two piercings in the cap: one to pass the tubing through and the other to provide an atmospheric vent. The vent piercings are made through the side of the cap and these are turned towards the rotation axis to prevent liquid loss from the vents during rotation.

The underside of the base unit (bottom view in Fig. 4) holds the chip, which is clamped with a composite element that also allows adjustment of the temperature field within the chip. This element consists of an outer aluminium collar and a lexan insert into which are embedded a copper heating ring and a central copper pin. The pin, ring, collar and lexan surfaces are each in direct contact with the chip undersurface. The base is otherwise constructed of PEEK so the top side of the chip is thermally insulated. The ring is wound with glass-coated nichrome wire (Pelican Wire Co., 35 AWG) to allow heat generation. The central pin is cooled using an air jet (not shown in Fig. 2). Thus, a radial temperature distribution is imposed on the chip, with low temperature in the centre rising to a peak in temperature at the heated ring and then decreasing to lower temperature at the collar. Significant heat is also generated in the motor windings and from slip ring friction. A water-cooled motor

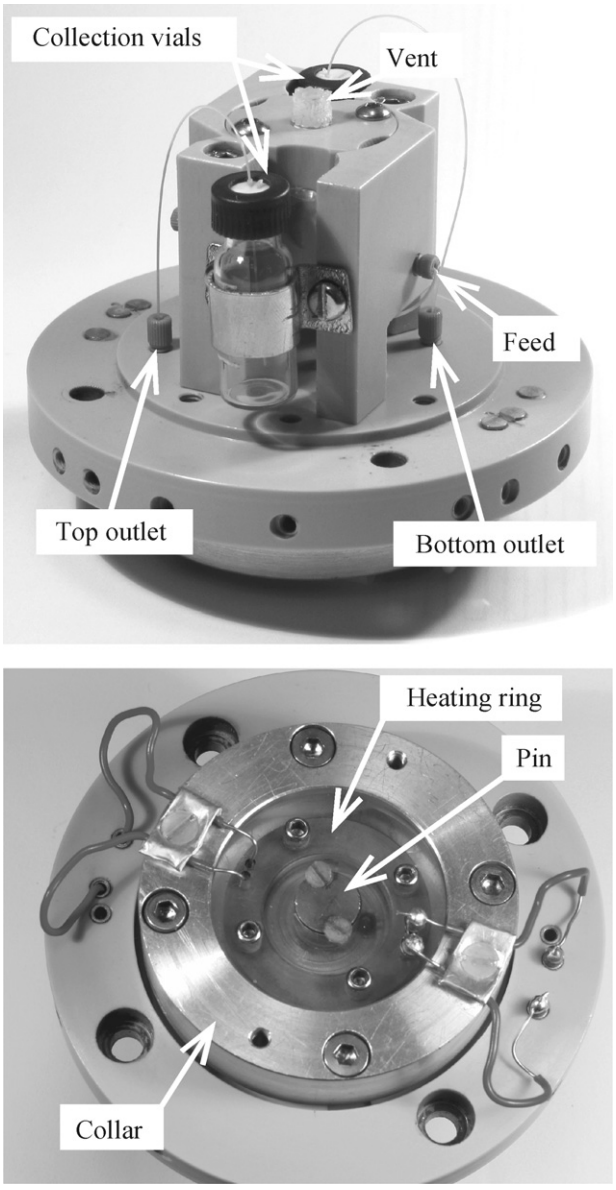

Fig. 4. Two views of the base unit showing (top) feed supply and product collection vials with connections through the base to the chip and (bottom) the thermal clamp element used to secure the chip and to control temperature field.

mount (Fig. 2) is used to limit heat flow down into the reservoir and chip regions.

Illumination for microscope imaging was from a strobe light transmitted through the objective lens and synchronised with the motor using a LabView (National Instruments) program. A reflective plastic film placed between the chip and the base allowed reliable visual detection of the liquid/vapour interface. Images were recorded using a monochrome charge coupled device camera.

In order to establish that the distillation state has been achieved, experimental determination of flow rates and compositions is required. The collection vial arrangement is designed to contain the collected liquid with negligible loss due either to leakage or to evaporation. The volumes collected from the bottom outlet will tend to be significantly smaller than those from the top outlet. (Simple mass balance for the experimental stripping process, Eq. (3), shows that the ratio of the top and bottom flow rates is much greater than unity for high bottom stream purity.) For this reason, while a standard vial bottle was suitable for the top flow, a vial with a small-volume insert was used to collect the bottom sample. As a

precaution against excessive sample evaporation, 100 μL of a high boiling point carrier liquid (*n*-heptane) was added to the top vial and 25 μL to the bottom vial prior to each run. Estimates of the mass transfer through the atmospheric vent suggest that less than 2% of collected liquid is lost by evaporation and that the liquid sample composition is altered by less than 0.2% as a result. Composition of the collected liquid in the two sample vials and that introduced to the feed reservoir was measured using gas chromatography (Varian 3900) with an estimated uncertainty of less than 2%.

2.2. Flow network design

Design of the contacting spiral and connecting channel details employs the relation between volume flow rate, *Q*, in a channel of size d and the driving centrifugal and pressure forces. Expressing average shear stress at the channel wall in terms of flow rate, channel size and fluid viscosity, the force balance in the *z* direction along the channel is, for developed flow:

$$\frac{dp}{dz} - \rho r\Omega^2 \sin\alpha = -\frac{f\mu Q}{Ad^2} \quad (1)$$

where α is the angle between the spiral channel and the tangential (θ) direction, Ω is angular velocity of rotation, r is distance from the rotation axis (Fig. 3) and A is channel section area. This is the usual Hagen–Pousielle result, but including the effect of centrifugal acceleration [33]. With no rotation and for single phase flow, the friction coefficient, f, is a constant for laminar flow depending only on channel section shape (e.g. $f = 32$ in the case of a circular section of diameter d) and can readily be determined (either analytically [34] or numerically [35]) for a given section shape. For a rotating channel, f can be altered by Coriolis secondary motion, the effect of which can be represented by the characteristic ratio of the secondary to the streamwise velocity. For low Reynolds number flow this ratio is given by the non-dimensional parameter $Ro = \rho\Omega d^2/\mu$ which is the Rossby number (alternatively the inverse Ekman number [11]). In the experiments here the Rossby number is expected to be sufficiently small for the secondary motions to have negligible effect on the friction coefficient and so f values for flow in stationary channels can be used directly.

Eq. (1) can be integrated along the channel to produce the required relation in terms of pressure and radius differences over a length of rotating channel, Δz. Noting that $\sin\alpha = dr/dz$, the result of this integration is

$$\Delta p - \frac{1}{2}\rho\Omega^2\,\Delta(r^2) = -\frac{f\mu Q}{Ad^2}\,\Delta z \quad (2)$$

The Δ operation signifies the difference between the value at the outlet and that at the inlet to the channel section concerned, so for example $\Delta(r^2) = r_{out}^2 - r_{in}^2$.

For the two-phase flow in the contacting spiral channel, Eqs. (1) and (2) continue to apply for each phase individually except that in addition to the shear stress at the rigid channel wall surface the shear stress exerted at the moving phase interface must be taken into account. For design purposes, this was done using a rough approximation for the interface shear force in terms of the average velocities and section dimensions of the individual phase flows. The resulting model for the contacting channel along with Eq. (2) for the other channels in the network allowed estimation of flow rates in terms of channel sizes, radial position of atmospheric liquid surface in each vial and in the feed reservoir and the fraction of the contacting channel section area occupied by the liquid phase, ξ, using standard flow network analysis techniques [36–38].

Eq. (2) can thus be used along with the modified versions for each phase in the contacting channel to design the flow network. In the channels with just liquid phase present (feed and outlet channels) Eq. (2) shows that even when the inlet and outlet pressures are equal, the pressure can vary along the channel depending on how r varies with z. Indeed, it is possible for the pressure to drop below the liquid bubble point pressure and for cavitation to occur, as has been demonstrated for a radial ($\alpha = \pi/2$) rotating channel [33]. In the case of the spiral contacting channel, a uniform state of flow along the entire length of the channel is desirable to maintain consistent contacting effectiveness. For either phase, the interface shear stress and the pressure gradient will be independent of distance along the channel for a fixed flow state. Eq. (1) then shows that centrifugal body force must remain constant along the spiral. Since density and rotation rate are independent of position along the spiral (gas density approximately so), uniform contacting along the spiral is achieved when $r\sin\alpha$ is constant. Thus, the spiral angle must decrease with increasing r and hence with distance along the spiral to maintain a constant body force.

It is noted that for the experimental conditions of flow in the contacting channel the liquid phase is driven primarily by centrifugal body force, while the vapour phase is driven primarily by pressure gradient. Further, the fraction ξ of the channel section area occupied by the liquid is small since the liquid is much denser than the vapour while molar flow rates of the two phases are similar. Thus, the thickness of the liquid layer in the contacting channel and the liquid flow rate are largely determined by rotation rate and spiral geometry ($r\sin\alpha$) and the vapour flow rate is largely determined by pressure gradient (since the liquid occupies a small fraction of the section area and its velocity is small). It is also noted that the pressure increase along the channel required to produce counter-current flow of the vapour gives a corresponding increase in the vapour density along the channel. For the experimental conditions, pressure is around 1 bar in the contacting channel but changes by about 0.1 bar over its length. Hence the vapour density is constant to within 10% in the experiment. For longer channels or higher flow rates account will need to be taken of vapour density and pressure variation, or greater section area will need to be used to reduce the pressure gradient along the spiral.

2.3. Thermal design

The temperature distribution throughout the chip must be precisely controlled if enrichment is not to be limited by the thermal conditions. As liquid flows outward along the spiral it must become enriched in the least volatile component. At approximately constant pressure, as is the case, this corresponds to a requirement of increasing temperature along the channel arising from thermodynamic equilibrium. In an adiabatic channel this increase in temperature would be produced by heat transfer from the interface caused by slight net condensation. However, at the small scale of the chip the spiral channel is far from adiabatic and the fluids in the channel may be expected to be close to the local chip temperature. In order to control fluid temperature along the channel, then, it is necessary to control the temperature distribution in the chip as a whole. Therefore, the temperature field along the contacting channel must increase going from the junction to the reboiler and must continue to rise into the re-boiling region so that sufficient heat transfer occurs to evaporate the liquid thereby supplying the counter-current vapour flow. Also, the temperature of the feed channel should remain below the bubble point of the feed mixture, reaching the bubble point temperature at the junction, where phase-contacting commences. Beyond the reboiler both product streams are condensed to allow liquid phase outlet flow and sample collection. For this to occur, temperature must drop to below the respective dew points beyond the re-boiling region and before the chip outlet positions are reached. These requirements are all satisfied by imposing an axisymmetric temperature field with temperature increasing radially from the rotation (spiral) axis to a maximum in the re-boiling region and then decreasing with radius

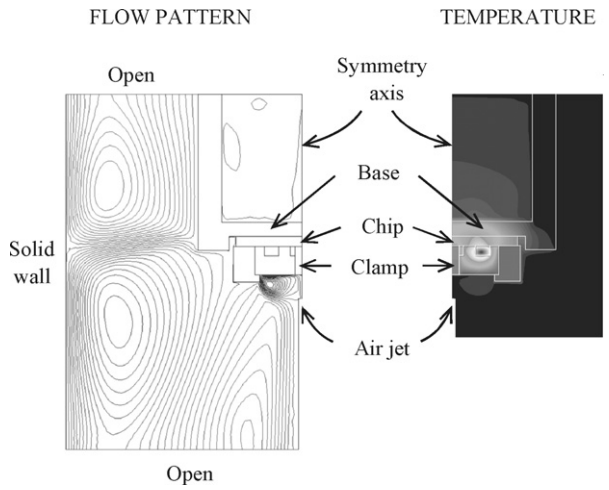

Fig. 5. 2D axisymmetric thermal model computation result for rotating condition. Stream function contours for velocity in the plane of the computation (left) and temperature contours throughout the device (right).

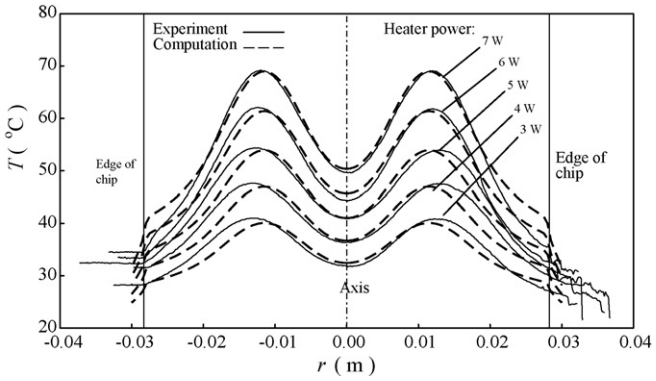

Fig. 6. Measured and computed temperature along a diagonal of the top surface of the chip with no rotation.

beyond this point to allow the necessary condensation for liquid outlet flows.

Computational studies were made in support of the apparatus design in which variously the equations for flow and heat transfer in both 2D and 3D representations of the design geometry were carried out (using Fluent, Version 6). The most useful level of representation was found to be a 2D axisymmetric approximation to the actual geometry, including both the conduction heat transfer within the solid regions comprising the main components surrounding the chip and the turbulent flow and heat transfer in the air adjacent to the apparatus. Including the flow in the surrounding air allowed reliable representation of convective heat loss from the device. The modelling employs the standard k–ε turbulence model [39] and includes the cooling jet flow and the effect of the moving solid surfaces of the rotating unit in driving flow in the adjacent air. The geometric domain employed can be seen in Fig. 5, where results of a computation for the rotating condition are shown. The cooling jet and the rotating surfaces of the unit induce strong convection in the air, which aids heat transfer to cool the chip centre through the copper pin and the periphery of the chip through the aluminium collar. This moderates the heater input at the ring to produce the desired rising and then falling temperature with radial position.

Before attempting to operate the device, it was desirable to determine what heater and cooling jet settings might be expected to produce a suitable temperature profile to allow successful distillation of a particular feed mixture. Measurements of the temperature produced in the actual device could not be made easily under the rotating condition of interest. Instead measurements were made with heating and cooling jet flow but without rotation to provide data to establish the reliability of the 2D computational model. The model could then be used to predict the temperature within the chip (at the level of the channels) for the rotating condition.

Temperature was measured using a K-type thermocouple formed by twisting the stripped ends of 75 μm diameter insulated chromel and alumel wires (Omega). This thermocouple was drawn along a diagonal of the top chip surface so that it travelled at a constant speed while temperature was continuously recorded. The thermocouple was guided by a slot formed from the gap between two pieces of 340 μm thick cardboard laid side-by-side on top of the chip. The thermocouple fitted snugly in the groove and could be drawn at a regular rate by winding it onto a slowly rotating spindle of known diameter and rotation rate.

Fig. 6 shows temperature profiles (solid lines) for a series of different heating rates measured in this way. Symmetry is good and the expected rising and then falling pattern of radial temperature distribution is observed. Plotted with the measured profiles are the corresponding predictions of the 2D computational model. Acceptable agreement with the measurements is found in the important region up to and including the peak temperature at the location of the heating ring. It is in this region that the feed channel and contacting spiral lie and the re-boiling must occur, and clearly the model is able to estimate temperature there quite accurately. At the peripheral regions of the chip agreement is poor, no doubt because the model is axisymmetric whereas the square shape of the chip (along with clamping bolts) spoils this symmetry at larger radii. The important characteristic of the peripheral temperature field is that temperature drops significantly below the respective dew points of the product mixtures. For lower levels of heating power the computational model underpredicts peripheral temperatures and thus overpredicts the capacity for condensation and this needs to be taken into account when interpreting the computed results.

Finally, the computation is used to predict temperature at the channel level in the chip under rotating conditions. The predicted result in Fig. 7 is for the same heating power, rotation rate and jet flow rate used in the experimental tests. The normal boiling points of the two pure components and the bubble point of the feed mixture are indicated by horizontal dashed lines for reference. Importantly, the junction is near the feed bubble point temperature, the outlet temperatures fall well below the respective dew-point values and the peak temperature (in the vicinity of the heating ring) exceeds the heavy-component boiling point.

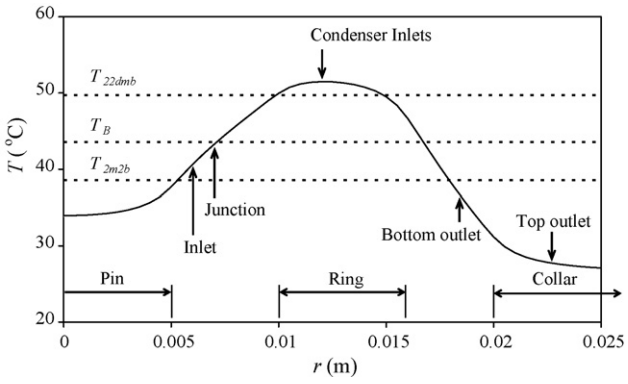

Fig. 7. Radial temperature profile at channel level under rotating condition predicted using the 2D axisymmetric thermal model. Jet flow rate, ring heating power and rotation rate are set to the values used for the experiment.

3. Results

3.1. Distillation operating state

Tests used a 50:50 (mol) feed mixture of 2-methyl-2-butene (2m2b) and 2,2-dimethylbutane (22dmb). Normal boiling points are 38.6 °C for 2m2b and 49.7 °C for 22dmb, so 22dmb is the heavy component and the one to be purified. Even with the temperature prediction of Fig. 7 it is not possible to predict reliably the flow rates that will occur. This is because the flows depend on the heat transfer rate to the liquid which determines the evaporation rate in the reboiler region. This evaporation raises the pressure there and consequently affects vapour flow directly and the flow of liquid indirectly. The flow of liquid in turn affects the heat transfer and an accurate representation of this coupled process is not yet available. Thus, some of the remaining parameters must be determined by trial and error. Rotation rate is selected to give good segregation of the phases to ensure that they flow in neat layers (this was estimated early on to be in the region of the value of 5000 rpm used here in the case of 100 μm channels and typical liquid density and surface tension). This leaves the radial positions of the feed liquid level and the outlets to the two collection vials to be chosen. Flow is not sensitive to feed liquid level since from Eq. (2) dependence is on the square of radial position and the radial position will be small compared with the outlet radial positions. Thus, trial and error was required to establish suitable positions for the remaining parameters: the radial position of the outlet feeding each of the two collection vials. Adjustment was made until satisfactory counter-current flow and multistage distillation was achieved, i.e. the phases flowed in layers along the contacting channel, significant product liquid collected from both outlets and marked increase in the bottom product 22dmb concentration relative to that in the feed.

The operating state identified used 5000 rpm, an initially full feed reservoir (radial position of feed level effectively zero), 4 W heater power, 0.23 L/s air jet flow rate and a top outlet position of r_T = 27 mm. With these settings, the relative flow rates from the top and bottom outlets could be varied by changing just the bottom outlet position, r_B (from 17 to 21.5 mm in the experiments). This adjustment corresponds to changing the amount of liquid evaporated in the re-boiling region, with increasing r_B allowing higher bottom product flow and correspondingly lower liquid evaporation rate. Fig. 8 shows photographs taken with the microscope during a run with r_B = 17 mm, i.e. a relatively high evaporation. The visible part of the chip is that between the central cooling pin and the heating ring and this area is represented by the cropped chip photograph at the centre of the figure. The photographs are from various positions along the contacting channel as indicated, starting from the junction ($\theta = 40^\circ$) and finishing at $\theta = 370^\circ$, where the contacting channel reaches the radial position (10 mm) corresponding to the inside radius of the heating ring. Beyond this radius the channel is no longer visible. This visible length of the contacting spiral (junction to where it meets the ring) is 53 mm. Thus, the nine images shown are at about 6 mm intervals along the spiral.

A number of important observations can be made with reference to Fig. 8. First of all, the liquid layer is clearly visible along the outer side of the channel. This liquid layer is found to be stable, steady and reproducible. As can be seen, the liquid layer width is not uniform, being thinner on one side of the spiral (images at $\theta = 90^\circ$, 135°, 175°) and thicker on the opposite side (images at $\theta = 270^\circ$, 305°, 340°). A survey of the geometry suggests this is probably the result of the spiral not being exactly centred relative to the rotation axis. The result of this offset is a relatively high value of $r \sin\alpha$ on one side of the spiral and a relatively low value on the other, i.e. the driving force for the liquid is precisely constant as intended. The survey indicates an offset of 340 μm in direction $\theta = 150^\circ$ giving a position of lowest $r \sin\alpha$ and, hence, thickest liquid layer at $\theta = 240^\circ$. This result is some 60° away from the region of maximum layer thickness (at around 310°), a difference which is probably due to error in determining the actual offset. A further observation concerning liquid layer thickness is the apparently rapid reduction between 340° and 370°. The contacting channel is very near to the ring position where chip temperature, according to Fig. 7, reaches the heavy-component boiling point and evaporation and re-boiling may therefore have become significant in that region.

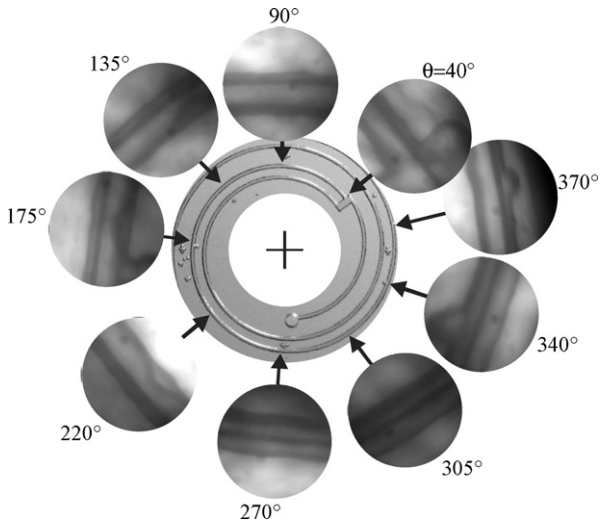

Fig. 8. Photographs taken during the distillation flow (r_B = 17 mm) at various positions along the contacting channel. The central image of the chip shows the visible portion and approximate positions of each photograph.

An observed feature of the contacting process is the generation of liquid droplets at the inner side of the contacting channel. Droplets grow and then disappear (presumably meeting and then very rapidly being drawn into the liquid layer along the outer side) in a repeating cycle. The droplets tend to emerge from particular sites along the inner channel surface, spaced at intervals of a few channel widths all along the contacting channel. Such droplets are captured in Fig. 8 in the images at $\theta = 135^\circ$, 175° and 220°, but could just as easily have been recorded in the images at other positions. The obvious explanation for the presence of these droplets is vapour condensation on the cooler inner channel surfaces resulting in a growing pendulous droplet which eventually becomes large enough to be pulled by the centrifugal force against the restoring surface tension force to join the flowing liquid layer at the outer channel surface. It seems likely that the droplet growth and direct addition to the liquid layer will tend to promote somewhat the equilibrium between liquid and vapour. A similar condensation effect occurs in the initial length of the vapour spiral, where from about 135° to 220° a liquid layer was observed, but with no liquid visible either before or after this section. This is consistent with the vapour moving initially in towards the axis from the junction (in order to meet the vapour spiral, Fig. 8), which of course places the vapour in contact with glass channel surfaces at temperatures below its dew point. It is not until $\theta = 167^\circ$ that the vapour spiral returns to the same radial position (and hence temperature) of the phase interface in the junction. An explanation is that condensation of the vapour stream beginning at the junction finally yields visible liquid at 135° and re-evaporation begins at around 167° and is not completed until beyond 220°.

3.2. Determination of product flow rates and compositions

Quantitative determination of the flow rates from the top and bottom outlets and the concentrations of these product streams

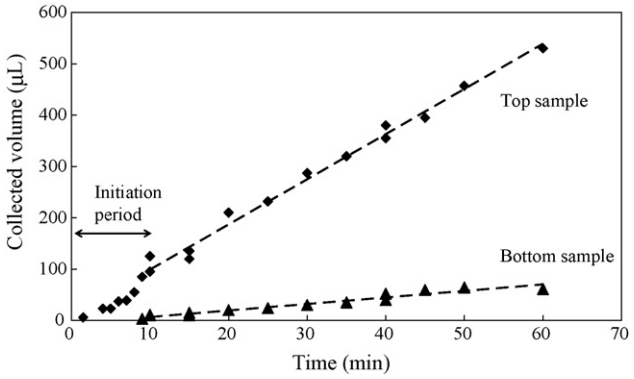

Fig. 9. Measurements of collected sample volumes when the experiment is stopped at different times using the same experimental conditions (r_B = 17 mm).

proved possible and the details of this are now given. By repeating a given test many times but stopping at different points in time, the volume and composition of the liquid collected in each vial could be determined as functions of time. Fig. 9 gives a typical result for collected volumes of product liquid from the top and bottom outlets, with time measured from the start of rotation. After an initiation period of approximately 10 min, the figure reveals linear increases in collected volume, i.e. constant flow rates. The initiation period is associated with the way the distillation flow was initiated. In each test, the apparatus was preheated using 8 W heater power for 10 min before the start of rotation. When rotation was initiated, heating was reduced to the 4 W value giving suitable chip temperature for distillation. Thus, during the initial period of rotation, chip temperature is adjusting due to the reduction in heating power and also to the changes in convective cooling associated with rotation. By 10 min after the start of rotation and reduction in heating, the temperature throughout the device has reached approximately steady state. Once the temperature field has become steady, reboiling of liquid becomes steady and mass transfer and species compositions throughout the device consequently become steady.

Fig. 10 shows the corresponding measured mole fractions of 22dmb (least volatile component) in the collected sample liquids, again as a function of time. In the bottom sample during the initiation period, too little is collected to allow accurate GC measurement, although composition can be measured for the top sample during this period. The collected material from the top shows that the mole fraction begins at the feed composition of 0.5, that of the feed mixture, and settles to a lower composition as expected for vapour in equilibrium with the feed mixture. The initial high temperature state resulting from the high preheating

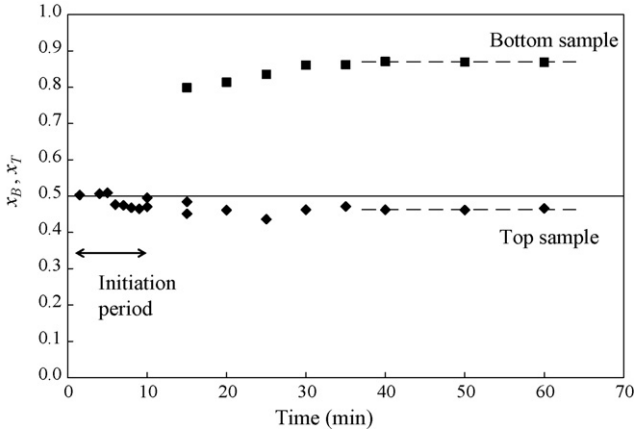

Fig. 10. Measured mole fractions for collected sample. Same tests as in Fig. 9.

Table 1
Results summary.

r_B (mm)	Q_B (nL/s)	Q_T (nL/s)	L_T/L_B	x_B	x_T
21.5	74.3	95.0	1.35	0.657	0.410
20.5	68.5	123	1.92	0.736	0.404
20.0	45.0	131	3.13	0.783	0.442
18.5	36.0	142	4.27	0.826	0.453
17.0	20.3	144	7.72	0.870	0.463

power results in fully vaporised flow on the chip and feed fluid passes equally from the top and bottom outlets. This initial vapour flow also serves to clear air from the channel network. Beyond the initiation period the mole fraction of the bottom sample shows an increase to an asymptotic level that is reached within the measurement accuracy in about 40 min. Since there is an initial deposition of mixture similar in composition to the feed during the initiation period and since the flow rate from the bottom outlet is subsequently small (Fig. 9) measured concentration is noticeably reduced at early times, requiring sufficient dilution by sample flow before the readings accurately reflect the steady state condition. Thus, for purposes of quantitative comparisons, the compositions prevailing during steady operation are taken as the average of measured values beyond 40 min and the flow rates are taken as the slope of the least-squared-error linear fit to the volume data beyond 10 min (indicated by dashed lines in Figs. 9 and 10).

The above procedure was repeated for the bottom outlet radial positions r_B = 18.5, 20.0, 20.5 and 21.5 mm. In each case, collected volume was linear with time beyond the initiation period, composition settled to an asymptotic value by 40 min and the visual character of the flow for a given case was reproducible. The results of all the tests are summarised in Table 1 and, as expected, moving the bottom outlet to larger radius increases the flow rate from the bottom and correspondingly decreases that from the top. Thus, the ratio of top and bottom (molar) flow rates, L_T/L_B, is made to decrease as r_B is increased. An overall mole balance on the heavy component shows that the bottom mole fraction depends on the feed and top mole fractions and the molar flow rate ratio:

$$x_B = x_F + (x_F - x_T)\frac{L_T}{L_B} \quad (3)$$

Since the mole fraction of the heavy component in the top vapour flow is lower than that of the feed liquid this equation shows that the bottom mole fraction of the heavy component must increase with increasing flow rate ratio. This is indeed found to be the case for the measurements (Table 1).

Some further characteristics of the distillation must be mentioned at this point. First, again associated with radial increase in temperature in the central region of the chip, it is found that a vapour pocket forms upstream of the junction in the feed channel. Fig. 11a shows this vapour pocket in the case of r_B = 17 mm. It was intended that the feed mixture remain liquid up to the junction where it first encounters vapour from the contacting spiral. However, with temperature gradient in the downward direction in the figure, the feed liquid clearly enters the junction through a region at slightly higher temperature than its bubble point and apparently allows some evaporation of the feed liquid and formation of the vapour pocket. The vapour pocket plays no role in the distillation flow since its composition remains steady and, judging by the thickness of the adjacent liquid layer, does not introduce significant flow resistance. The liquid feed channel could have been routed into the junction differently to avoid this bubble.

A second observation concerns the stability of the flow states of the conditions tested. As the bottom outlet is moved to larger radial position, the flow develops increasingly strong oscillatory character. For r_B = 17, 18.5 and 20.0 mm increasing oscillation of the vapour pocket just described is observed, but with no apparent

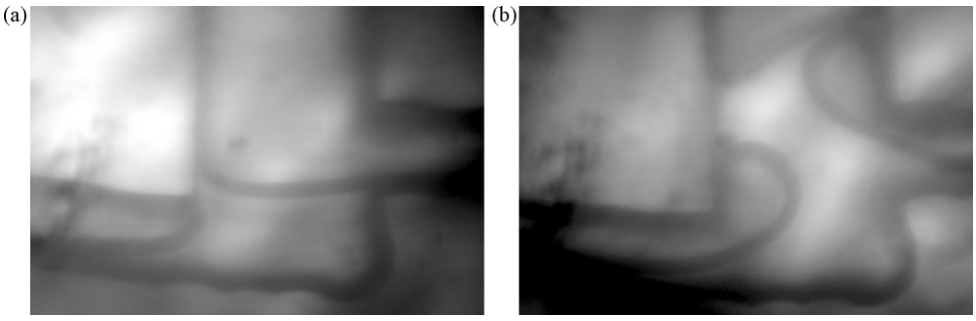

Fig. 11. Images taken at the junction for (a) r_B = 17 mm and (b) r_B = 21.5 mm. Stable flow is present in (a) while intermittent flow occurs in (b).

effect on the contacting flow. By r_B = 20.5 mm, significant disruption of the junction interface at regular intervals throughout the test takes place, with some liquid ejected upwards from the junction into the vapour flow and with waves of liquid being sent down the contacting channel. Fig. 11b shows an instant in this intermittent disruption during an r_B = 21.5 mm test. These large r_B cases have a reduced vapour flow rate and, hence, re-boiling requirement. No adjustment of heating was made as r_B was increased and it is likely that reduced heating is required to produce satisfactory flow in these cases.

3.3. Determination of the number of stages of separation

The number of equilibrium stages, N_e, produced by the device can now be estimated. One stage corresponds to the length of the contacting spiral channel required for the bulk concentrations of exiting liquid and vapour to correspond to an equilibrium state. Constant relative volatility and equal molar enthalpies of vaporisation for the species in the binary mixture are assumed. For the stripping distillation considered in the experiments, the molar flow rates of vapour and liquid remain constant along the contacting channel and are equal to the top and feed flow rates, respectively. (Constancy of flow rates is strictly true only when net heat transfer to the contacting channel is zero.) This results in a single flow parameter, taken to be the molar flow rate ratio L_T/L_B, determining outlet concentrations. For constant relative volatility, α, the heavy-component mole fraction of the vapour, y_n, leaving stage n can be expressed in terms of the liquid mole fraction of the heavy-component leaving the same stage, x_n, using the ideal mixture result:

$$y_n = \frac{x_n}{\alpha - (\alpha - 1)x_n}, \quad n = 0, N_e \tag{4}$$

This equilibrium applies equally to the re-boiling channel section (n = 0) which produces evaporation to supply the vapour counterflow and to the N_e contacting stages (n = 1, N_e). Note that the stages are counted from the re-boiling section inward along the spiral until the final stage (n) is reached just before the junction. Mole balance on the channel from each stage n out to the bottom outlet gives the N_e further equations:

$$x_{n+1} = \frac{x_B + y_n L_T/L_B}{1 + L_T/L_B}, \quad n = 0, N_e - 1 \tag{5}$$

Finally, the set of equations is closed by an overall balance which gives an equation for x_B in terms of the given feed mole fraction x_F:

$$x_B = x_F \left(1 + \frac{L_T}{L_B}\right) - \frac{y_{N_e} L_T}{L_B} \tag{6}$$

These 2(N_e + 1) equations uniquely determine the unknown stage compositions (x_n, y_n), n = 0, N_e given x_F, N_e and L_T/L_B. Antoine equation representation of pure component vapour pressures is used to determine the relative volatility as α = 1.45 for the binary pair considered, a value found to be constant to within about 0.2% over the entire composition range and over the pressure range along the contacting channel estimated for the experiment.

Fig. 12 compares the experimental data and solutions to the above model equations for 5, 10 and 15 equilibrium stages and for the experimental feed composition (x_F = 0.5) as a function of L_T/L_B. Generally, both the measured top and bottom compositions are in good agreement with the trend of the model. For L_T/L_B > 3 the model results suggest that between 7 and 15 equilibrium stages are achieved by the apparatus, the number of stages decreasing with L_T/L_B. The error bars show the estimated experimental uncertainty of approximately 13%, which is due principally to the determination of flow rates from the volume measurements. The error is not enough to account for the impossibly high purity measured for the two lowest L_T/L_B experiments. A somewhat higher value of 0.52 for the feed mixture mole fraction brings the model into agreement with these low L_T/L_B data. However, it is unlikely that the feed deviated this much from the intended value of 0.5. (Direct measurements of the feed reservoir liquid just before the start of each run gave values within 1% of the intended composition.) The cause of the too high purity values may be the oscillatory flow state mentioned previously that prevailed throughout the two tests concerned. If the flow is thought of as alternating between two modes, one with high flow rate ratio producing high purity and the other with low flow rate ratio producing low purity, then it is possible for the overall sample purity to be different from the value expected for a steady flow at the ratio of the average flow rates recorded for the test.

The most important outcome of the work is the demonstration that rotating spiral contacting has successfully produced distillation corresponding to multiple stages. Interpolation of results of the stage model indicates that the case with greatest reboil rate

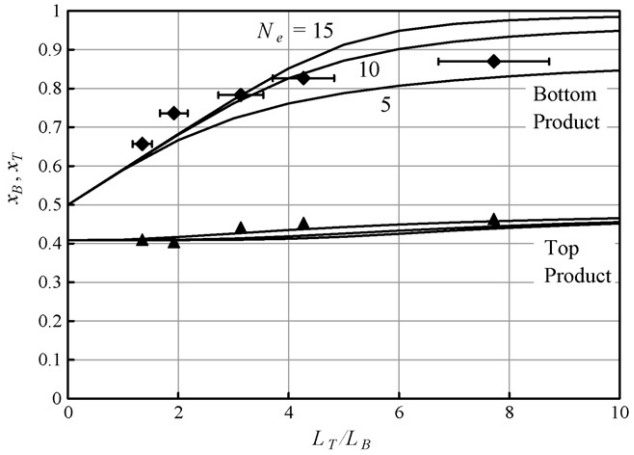

Fig. 12. Comparison with equilibrium stage model.

Table 2
Contacting conditions and performance parameters for some reported microchannel distillation devices.

	Zhang et al. [4]	Tonkovich et al. [2]	Present work
Contacting method	Membrane	Falling film	Rotating spiral
Mixture	Methanol, water	Hexane, cyclohexane	2-Methyl-2-butene, 2,2-dimethylbutane
h (μm)	72	178	50
u (mm/s)	1.2	1	40
D (m^2/s)	2×10^{-9}	5×10^{-9}	5×10^{-9}
ℓ (mm)	150	8.3	5.3
$\tau = \ell/u$ (s)	130	8.3	0.13
ℓ/ℓ_0	38	1.3	0.26

($L_T/L_B = 7.72$ corresponds to 6.6 stages of distillation. This is for a contacting length of 35.3 mm, the length along the spiral channel from the junction to the point along the channel where the temperature reaches the bubble point for the bottom product composition ($x_B = 0.87$). Using this overall length, the length of channel corresponding to one stage of distillation is found to be 5.3 mm.

3.4. Comparison with previous multistage microdistillation devices

To help place the present results into context, comparison is now attempted with the alternatives of membrane and falling film contacting. Just two studies provide quantitative results for counter-current distillation in a microchannel device: the membrane contacting reported by Zhang et al. [4] and the falling film contacting reported by Tonkovich et al. [2]. Thus, there is little data with which to compare at this stage and considerable work is required before the benefits of each approach can be fully clarified. However, it may be helpful to give a rough comparison here of the performance achieved with the various devices reported so far. As mentioned, the present rotating spiral channel device has produced an estimated 6.6 stages and a stage length of 5.3 mm. The membrane device used a microchannel length of 260 mm to produce just 1.7 stages, giving a stage length of 150 mm [4]. The falling film device produced separation corresponding to 15 stages with a stage length of just 8.3 mm [2]. Certainly a short channel length to reach one stage of distillation is important, but is this the appropriate parameter for direct comparison? An order of magnitude estimate of the stage length, ℓ_0, in terms of velocity, u, channel size, h, and diffusivity, D, results from equating convection and diffusion of species:

$$\ell_0 = \frac{uh^2}{D} \tag{7}$$

This could be determined for the properties and conditions of either phase but here just the liquid phase will be considered to simplify the discussion. From this relation, the reduction in stage length with channel size is evident. Decreasing channel size reduces both stage length and time, $\tau_0 = \ell_0/u$; decreasing velocity also reduces stage length (while also lowering the throughput). Table 2 summarises the conditions for the reported membrane, falling film along with those of the present rotating spiral contacting device. The velocity and channel size values given are for liquid velocity and liquid layer thickness in each case. The actual stage length values, ℓ, listed in the table are not directly helpful in making a comparison since these may merely reflect differences in flow rate, diffusivity or channel size according to Eq. (7). Even so, all three devices use similar channel size and involve liquids giving similar diffusivity. On the other hand, the stage length of the rotating spiral and falling film are much shorter than for the membrane device and the liquid velocity in the rotating spiral tests is much higher than for the other two devices.

To make a fair comparison the stage length relative to that expected from Eq. (7), i.e. ℓ/ℓ_0, should be considered and the estimated value in each case is listed in the final row of the table. The rotating spiral has given a stage length that is relatively small compared to that expected, that for the falling film is just about the expected value and in the case of the membrane device the stage length is much larger than expected. In the case of the rotating spiral, it might be expected that Eq. (7) overestimates stage length since it takes no account of the Coriolis secondary (Fig. 1) motion and this may explain the smaller relative stage length compared to that for the falling film. In the case of the membrane device, the large relative stage length must indicate some major problem with the device or the way it has been operated. There could be problems with flow, pressure or thermal control. Processing time for one stage, which can be taken as $\tau = \ell/u$, is a second important indicator of performance. Again, its ratio with the expected time τ_0 allows fair comparisons to be made and one can see that this ratio is exactly the same as for stage length, so comments concerning relative stage length apply equally to relative stage time. Actual stage times for the different cases are listed in Table 2 and those for the rotating spiral device tested here are far shorter than for the other two devices. Not only is the stage length shorter for the rotating spiral device but the liquid velocity achieved is about 40 times greater than in the other two devices.

It is emphasised that these comparisons are rough and depend on just one example of each type of device. Further work is needed before fundamental performance differences for the various approaches to microchannel contacting can be established conclusively. Still, rotating spiral contacting appears clearly to perform well, delivering both an efficient use of channel length (small ℓ/ℓ_0) and reduced processing time. While the demonstration device has produced around seven stages of distillation, the rotating spiral approach should in principle enable a much larger number of stages. The contacting channel can be considerably lengthened using multiple revolutions of the spiral with reduced spiral angle to achieve a compact device. It is also possible to increase the number of stages by decreasing flow rate. Making the device larger increases the rotation Reynolds number which is known to increase the effect of the Coriolis secondary motion [11], thereby decreasing the relative stage length. Thus, there is considerable scope for improving the technology and increasing the number of equilibrium stages. For example, simply increasing the channel length of the present device to 1 m using the same channel and flow parameters may be expected to give in excess of 100 stages of distillation judging by the results of the present work. There are a number of technical challenges that remain to be addressed. These include developing schemes (such as rotating seals) to allow fluid to be transferred continuously between the rotating unit and the stationary laboratory frame, so that continuous processing becomes possible. Another important issue, as has been mentioned, is achieving precise alignment of the spiral with the rotation axis.

4. Conclusions

Distillation in a rotating spiral microchannel has been demonstrated experimentally using a prototype device. A binary feed

mixture of 50:50 (mol) 2,2-dimethylbutane and 2-methyl-2-butene has been distilled to give a product containing 87% (mol) of the higher boiling component. Equilibrium stage theory indicates that 6.6 stages of distillation have been achieved and it is estimated that each stage requires 5.3 mm of channel length and distillation time is just 0.13 s per stage. Comparison with the results of other microchannel distillation devices reported in the literature suggests the rotating spiral has produced a more efficient contacting and more rapid separation. While further work remains in order to bring rotating spiral distillation into a practically useful form, the results demonstrate the essential feasibility of the approach.

Acknowledgements

The authors gratefully acknowledge financial support from the University of Sheffield OCP Proof of Concept Fund (Project 23039) and from the Mexican Government.

References

[1] C.R. Wootton, A.J. deMello, Continuous laminar evaporation: micron-scale distillation, Chemical Communications (2004) 266–267.
[2] A.L. Tonkovich, K. Jarosch, R. Arora, L. Silva, S. Perry, J. McDaniel, F. Daly, B. Litt, Methanol production FPSO plant concept using multiple microchannel unit operations, Chemical Engineering Journal 135S (2008) S2–S8.
[3] R.L. Hartman, H.R. Sahoo, B.C. Yen, K.F. Jensen, Distillation in microchannel systems using capillary forces and segmented flow, Lab on a Chip 9 (2009) 1843–1849.
[4] Y. Zhang, S. Kato, T. Anazawa, Vacuum membrane distillation on a microfluidic chip, Chemical Communications (2009) 2750–2752.
[5] W.J. Moore, Physical Chemistry, 4th ed., Prentice-Hall, New Jersey, 1972.
[6] W.L. McCabe, J.C. Smith, P. Harriott, Unit Operations of Chemical Engineering, 5th ed., McGraw-Hill, New York, 1993.
[7] J.L. Meriam, Dynamics, 2nd ed., John Wiley & Sons, New York, 1971.
[8] H. Miyazaki, Combined free and forced convection heat transfer and fluid flow in a rotating curved circular tube, International Journal of Heat and Mass Transfer 14 (1971) 1295–1309.
[9] H. Ishigaki, Laminar convective heat transfer in rotating curved pipes, JSME International Journal Series B 42 (3) (1999) 489–497.
[10] G.H. Lee, J.H. Baek, A numerical study of the similarity of fully developed laminar flows in orthogonally rotating rectangular ducts and stationary curved rectangular ducts of arbitrary aspect ratio, Computational Mechanics 29 (2002) 183–190.
[11] A.A. Draad, F.T.M. Nieuwstadt, The Earth's rotation and laminar pipe flow, Journal of Fluid Mechanics 361 (1998) 297–308.
[12] C.G. Speziale, S. Thangam, Numerical study of secondary flows and roll-cell instabilities in rotating channel flow, Journal of Fluid Mechanics 130 (May) (1983) 377–395.
[13] K.S. Yang, J. Kim, Numerical investigation of instability and transition in rotating plane poiseuille flow, Physics of Fluids A—Fluid Dynamics 3 (4) (1991) 633–641.
[14] L. Wang, Effect of spanwise rotation on centrifugal instability in rotating curved non-isothermal flows, Computational Mechanics 19 (1997) 420–433.
[15] H. Iacovides, B.E. Launder, Turbulent momentum and heat transport in square sectioned ducts rotating in orthogonal mode, Numerical Heat Transfer 12 (4) (1987) 475–491.
[16] H. Iacovides, B.E. Launder, H.-Y. Li, The computation of flow development through stationary and rotating U-ducts of strong curvature, International Journal of Heat and Fluid Flow 17 (1) (1996) 22–33.
[17] J.M. MacInnes, G.H. Priestman, R.W.K. Allen, A spinning micro-channel multiphase contactor, in: Seventh World Congress of Chemical Engineering, Glasgow, Scotland, July 10–14, 2005 (Congress Manuscript O120-001).
[18] M. Keyvani, N.C. Gardner, Operating characteristics of rotating beds, Chemical Engineering Progress (September) (1989) 48–52.
[19] S. Munjal, M.P. Dudukovic, P. Ramachandran, Mass-transfer in rotating packed beds—II. Experimental results and comparison with theory and gravity flow, Chemical Engineering Science 44 (1989) 2257–2268.
[20] T. Kelleher, J.R. Fair, Distillation studies in a high-gravity contactor, Industrial and Engineering Chemistry Research 35 (1996) 4646–4655.
[21] Y. Ito, Countercurrent chromatography, Journal of Biochemical and Biophysical Methods 5 (1981) 105–129.
[22] Y. Ito, Toroidal coil planet centrifuge for counter-current chromatography, Journal of Chromatography 192 (1980) 75–87.
[23] D.C. Duffy, H.L. Gillis, J. Lin, N.F. Sheppard, G.J. Kellogg, Microfabricated centrifugal microfluidic systems: characterization and multiple enzymatic assays, Analytical Chemistry 71 (20) (1999) 4669–4678.
[24] M.J. Madou, G.J. Kellogg, The LabCD (TM): a centrifuge-based microfluidic platform for diagnostics, Proceedings of the Society of Photo-Optical Instrumentation Engineers (SPIE) 3259 (1998) 80–93.
[25] J. Ducrée, I. Glatzel, T. Brenner, R. Zengerle, Coriolis-induced Flow Control for Micro- and Nanofluidic Lab-on-a-Disk Technologies, International Forum on MicroNano Integration, Potsdam, Germany, 2003.
[26] F. Yang, Y. Ito, Method for the fractionation of dextran by centrifugal precipitation chromatography, Analytical Chemistry 74 (2) (2002) 440–445.
[27] S. Haeberle, T. Brenner, R. Zengerle, J. Ducrée, Centrifugal extraction of plasma from whole blood on a rotating disk, Lab on a Chip 6 (6) (2006) 776–781.
[28] K. Jähnisch, M. Baerns, V. Hessel, W. Ehrfeld, V. Haverkamp, H. Löwe, Ch. Wille, A. Guber, Direct fluorination of toluene using elemental fluorine in gas/liquid microreactors, Journal of Fluorine Chemistry 105 (2000) 117–128.
[29] K.K. Yeong, A. Gavriilidis, R. Zapf, V. Hessel, Experimental studies of nitrobenzene hydrogenation in a microstructured falling film reactor, Chemical Engineering Science 59 (2004) 3491–3494.
[30] M. Zanfir, A. Gavriilidis, C. Wille, V. Hessel, Carbon dioxide absorption in a falling film microstructured reactor: experiments and modeling, Industrial and Engineering Chemistry Research 44 (2005) 1742–1751.
[31] J. De Jong, R.G.H. Lammertink, M. Wessling, Membranes and microfluidics: a review, Lab on a Chip 6 (2006) 1125–1139.
[32] S.H. Cypes, J.R. Engstrom, Analysis of a toluene stripping process: a comparison between a microfabricated stripping column and a conventional packed tower, Chemical Engineering Journal 101 (2003) 49–56.
[33] T. Maruyama, T. Maeuchi, Centrifugal-force driven flow in cylindrical microchannel, Chemical Engineering Science 63 (2008) 153–156.
[34] F.M. White, Viscous Fluid Flow, McGraw-Hill, New York, 1974.
[35] J.M. MacInnes, X. Du, R.W.K. Allen, Prediction of electrokinetic and pressure flow in a microchannel T-junction, Physics of Fluids 15 (7) (2003) 1992–2005.
[36] J.M. MacInnes, X. Du, R.W.K. Allen, Dynamics of electroosmotic switching of reacting microfluidic flows, Chemical Engineering Research and Design 81 (A7) (2003) 773–786.
[37] J.M. MacInnes, Modelling pressure and electrokinetic flow in complex microfluidic devices, microfluidics: history, theory and applications, in: W.B.J. Zimmerman (Ed.), CISM Lecture Series, vol. 466, Springer-Verlag, Wien, 2006, pp. 49–103.
[38] H. Bruus, Theoretical Microfluidics, Oxford University Press, Oxford, 2008.
[39] B.E. Launder, D.B. Spalding, The numerical computation of turbulent flows, Computational Methods in Applied Mechanics and Engineering 3 (1974) 269–289.